Cold Regions Science and Technology 165 (2019) 102795

Contents lists available at ScienceDirect

Cold Regions Science and Technology

journal homepage: www.elsevier.com/locate/coldregions

Finding safe and efficient shipping routes in ice-covered waters: A framework and a model

Ville Lehtola[a,b,*], Jakub Montewka[a,c], Floris Goerlandt[d,e], Robert Guinness[a], Mikko Lensu[f]

[a] Finnish Geospatial Research Institute FGI, National Land Survey of Finland, PO Box 84, 00521 Helsinki, Finland
[b] University of Twente, ITC faculty, EOS department, Enschede, the Netherlands
[c] Gdynia Maritime University, Department of Transport and Logistics, Gdynia, Poland
[d] Aalto University, Department of Mechanical Engineering, Marine Technology, PO Box 15300, FI-00076 AALTO, Finland
[e] Dalhousie University, Department of Industrial Engineering, Halifax, Nova Scotia B3H 4R2, Canada
[f] Finnish Meteorological Institute FMI, PO Box 503, 00101 Helsinki, Finland

ARTICLE INFO

Keywords:
Ice navigation maritime safety
Route optimization
Geo-information
Multi-objective optimization
Pathfinding

ABSTRACT

Safety for conventional and autonomous navigation in ice-covered waters is a topic of rising importance. Here, we propose a generic extendable framework to provide the optimal route from multiple route planning objectives. These objectives are attained by an evaluation of multi-source input data, including state-of-the-art model data for ice conditions, for bathymetric knowledge, and for ship-ice interaction. Additionally, we model the ship-ship interactions statistically using a mean-field, to account for ships (indirectly) assisting each other via artificial ice channels. For the subsequent pathfinding problem, we propose a new A*-based algorithm that yields output which is not dependent on the grid format of the input data but instead consists of a path that follows the Earth's curvature. The outputs of the algorithm are a set of waypoints (representing the optimal route), the travel costs (expressed in time), and the additional travel cost estimates caused by route deviation, should the optimal route be altered in any way. The steaming speeds, the optimal route, and the deviation times are represented with two-dimensional (2D) maps. Finally, we provide a model implementation of our framework as a Matlab-package, ICEPATHFINDER, that is suitable for both operational and strategic ship route optimization.

1. Introduction

Ice navigation is essential for many countries, e.g. Finland (Lépy, 2013), and has major application potential if new shorter routes open in the Arctic as global temperature raises (Lasserre and Pelletier, 2011; Valkonen and Riska, 2014; Kum and Sahin, 2016; Aksenov et al., 2017; Beveridge et al., 2016). Hence, ice navigation tools gather interest from two directions. First, the safety perspective aims to keep the risks to life, property, and the environment at levels which are as low as reasonably possible (Kum and Sahin, 2015; Fu et al., 2016; Khan et al., 2018; Barabadi et al., 2015; Bye and Aalberg, 2018). Second, the automation of ships is taken further by gathering and processing data for decision making (Kotovirta et al., 2009; Choi et al., 2015; Guinness et al., 2014; Montewka et al., 2015; Kuuliala et al., 2017; Zvyagin and Voitkunskaia, 2016; Schütz et al., 2014; Dong et al., 2016).

The planning of safe routes is essential in ice-covered waters for several reasons. Statistical data analysis indicates that accidents occur more frequently there than in open-water conditions (Kum and Sahin, 2015; Goerlandt et al., 2017a, 2017b). Moreover, these accidents can have severe consequences, especially in terms of damage to the environment, as indicated by a risk analysis of maritime accidents in ice-covered waters (Valdez~Banda et al., 2015). Polar areas are fragile, and it is challenging to clean-up the contamination that may follow an accident (Lu et al., 2019; Khan et al., 2018). In order to ensure the safety of navigation in ice-covered waters, extensive regulatory frameworks at various levels have been developed to manage the risks. A few examples are the rules governing the Finnish-Swedish Winter Navigation System (FSWNS) at regional level (Riska, 1997) and the global Polar Code (Ghosh and Rubly, 2015). Apart from stipulating ship design requirements, e.g. in terms of required plate thicknesses to withstand ice loads or the required engine power to overcome ice resistance, several operational requirements are also implemented. For instance, the FSWNS imposes traffic restrictions to vessels in terms of minimum tonnage and ice class when visiting certain ports, depending on the ice conditions (Valdez Banda et al., 2015). The Polar Code similarly contains provisions concerning operational limitations of vessels in

* Corresponding author at: Finnish Geospatial Research Institute FGI, National Land Survey of Finland, PO Box 84, 00521 Helsinki, Finland.
E-mail address: ville.lehtola@iki.fi (V. Lehtola).

https://doi.org/10.1016/j.coldregions.2019.102795
Received 14 September 2018; Received in revised form 10 April 2019; Accepted 2 June 2019
Available online 05 June 2019
0165-232X/

different ice regimes, making use of the Polar Operational Limit Assessment Risk Indexing System (POLARIS); see e.g. Stoddard et al. (2016).

Another characteristic feature of ship navigation in ice conditions is the different modes of operations in which vessels proceed on their journey. Two fundamental modes are commonly distinguished: independent and icebreaker-assisted navigation (Rosenblad, 2007). In the former, a vessel navigates using her own power through the ice fields with ship officers responsible for planning and executing the route in light of the prevailing ice condition. In the latter, a merchant vessel is assisted by an icebreaker, which provides guidance to the officers while facilitating the physical process of making the passage through the ice fields. Five icebreaker assistance operations can be distinguished: escorting, convoy, double convoy, towing, and breaking a ship loose (Goerlandt et al., 2017b). This division omits that in reality a ship following the path of another (commercial) ship may receive indirect aid for steaming in the ice-covered waters, e.g. if an ice channel stays open. Unless this (indirect) interaction between the ships is explicitly added to the route planning, there is a discrepancy between the computational routing tools and reality, because rooting tools otherwise simplify the real-world conditions by assuming that the considered vessel is the only one navigating in the area.

Independent navigation is considered the most challenging wintertime navigational operation, from the perspective of both ice-breaker and merchant vessel, as the results of interview among ice navigation professionals reveal (Jalonen et al., 2005; Boström and Österman, 2017). Furthermore, a recent risk analysis of winter navigation in Baltic Sea ice conditions shows in particular that independent navigation and convoy operations involve a high risk of collision and subsequent economic losses (e.g. ship damage, delays) and environmental damages (Valdez Banda et al., 2016). That analysis also suggests that the navigational risks can be reduced significantly through the development and implementation of e-Navigation services, such as tools for supporting route planning through ice fields.

In this paper, we therefore intend to improve the safety of winter navigation by providing a navigator (or autonomous ship) the optimal route, i.e. the fastest and the safest route, in given anticipated ice conditions. Our algorithm also provides the additional cost (in time) that would be incurred by deviating from the estimated optimal route. The contribution to the state-of-the art is made in four ways, as discussed below.

First, we formulate a framework that can incorporate multiple data sources and multiple pathfinding objectives. This is important, since navigation in ice covered waters is very challenging, and therefore in reality, all available knowledge and information is applied to support the navigational decision making. Here we employ the following information: (1) attainable speed of the ship resulting from (2) the surrounding time-dependent ice conditions, (3) the probability of a ship besetting in ice, (4) the modified speed due to the likelihood of other ships being present in shipping routes, and (5) bathymetry. In addition, our bathymetry algorithm allows for the exclusion of narrow waterways which shall be avoided by ships navigating independently in ice as stipulated by the FSWNS.

Second, the concepts of a speed map and an (integrated) steaming time map are introduced to provide estimates about the accuracy of the optimal route for safety purposes. Compared against the state-of-the-art, the time map is a new concept that answers to a need to have the ability to conveniently estimate travel times knowing that route modifications are probable. We also discuss the connection between the speed map and the typically employed ice maps.

Third, in order to dissolve the contradiction between reality and the assumption that the ship is navigating alone on the sea, the (indirect) interaction between the ships via artificial ice channels must be taken into account. This has not been done before. We propose a new ship-ship interaction model via a so-called *mean-field* (see e.g. Le Boudec et al., 2007). The mean-field is integrated in the proposed framework and derived from historic AIS data.

Fourth, our pathfinding algorithm is designed and implemented so that it can model entire shipping routes. These routes given as output are physically realistic geodesic paths, i.e. they relax the spatial discretization of the input data. Our Matlab implementation, ICEPATHFINDER, can process the Baltic Sea with state-of-the-art weather data using a sub-nautical mile resolution in a reasonable computational time. To the best of our knowledge, our method is the most accurate one at this length scale.

The method presented here is generic. However, the case study presented relates to the Baltic Sea, which offers a significant amount of data on maritime traffic in ice. The ice conditions vary, both temporally and spatially from winter to winter. In case of a harsh winter, more than half of the basin can be covered by various formations of ice, including ridges. These ice fields, especially the ridged ones, can experience severe compression that significantly hamper ice navigation. In case of a light winter, only northern parts of the Baltic Sea experience ice, while the rest of the area remains open (Löptien and Dietze, 2014).

The rest of the paper is organized as follows. First, we discuss the related work (Section 2), and then we propose our method (Section 3). Thereafter, we introduce the data (Section 4) for which we present the results (Section 5). Finally, we discuss the results (Section 6) and summarize our work in the Conclusion (Section 7).

2. Related work

This section gives an overview of the relevant approaches to determine ship performance in ice-covered waters, as well as the tools suitable for routing vessels through these waters.

2.1. Ship performance in ice

In order to estimate the vessel transit speed in different ice regimes, a model for ship performance in ice is normally employed. The purpose of such a model is to estimate the attainable speed of a vessel based on characteristics of both the ice field and the ship. We characterize these models into two types: semi-empirical (simulation) models, and data-driven models.

Semi-empirical models are based on an analytical breakdown of resistance components. Each of these is modeled using either an analytical, an empirical, or a combined approach. Several such models have been proposed for level ice (Lindqvist, 1989; Riska, 1997), and ridged and channel ice (Mellor, 1980; Riska, 1997). For a comprehensive overview see Erceg and Ehlers (2017). Simulations focus on detailed modeling of the impact of ice loads on the hull. The most relevant physical processes, i.e. ice crushing, bending, rotation, and submergence, are modeled on different parts of the hull. Local loads are aggregated over the whole ship hull in the time domain, from which the overall ship resistance and, when combined with thrust estimation, the ship speed is determined. There are models developed for level ice conditions (Liu et al., 2006; Lubbad and Løset, 2011), and for ridges Kuuliala et al., 2017; Gong et al., 2017). For a recent literature review see (Li et al., 2018).

Data-driven models do not capture the physical processes of ship-hull interaction, but rather tend to mimic the dependencies between ship speed and/or the probability of the vessel getting beset in ice, i.e. becoming unable to move. To this end, some combination of data sources is used, typically including ship speed data (often from the Automatic Identification System - AIS) and ice data (hind-cast data from operational sea ice prediction models or ship-borne measurement devices). Such models have been proposed for the Baltic Sea (Montewka et al., 2015), and for Arctic areas (Fu et al., 2016; Kubat, 2012; Mussells et al., 2017).

Considering the strengths and weaknesses of each of these modeling approaches, a hybrid model for ship performance in ice has been proposed specifically for use in route planning methods, see (Montewka

Table 1
Summary of existing ice routing tools (N/S, not specified; N/A, not applicable).

Year, author	Routing algorithm	Spatial and temporal resolution	Ship performance model	Source of ice data	Application area
2003, Frederking	Manual	> 10 × 10 NM, 1 day	Engineering based model, level ice, ridged ice included, taken from Keinonen et al., 1991	Ice egg from Canadian Ice Service	Ship operations, travel time & fuel consumption in the Gulf of St.Lawrence
2009 Kotovirta, et al.	Powell's method	1 × 1 NM, 6 h	Engineering based model, level ice, ridged ice included, taken from (Riska, 1997)	Ice model HIROMB	Ship operations & route optimization for the Baltic Sea
2013, Nam et al.	A*	20 × 20 NM, 1 month	Factors multiplied design speed for ridged ice and compressive ice	Ice model	Strategic planning & route optimization for Arctic Sea
2013, Choi et al.	Genetic algorithm	20 × 20 NM, N/A	Engineering based model, min/max speed for level ice	Ice model Ice-POM	Strategic planning & route optimization for the Arctic Sea
2014, Takagi et al.	Probabilistic roadmap, Dijkstra	Size of ice floes, N/A	No speed info, distribution of ice floes	Ship's radar	Ship operations & route optimization for short ranges
2014, Guinness et al.	A*	1 × 1 NM, 6 h	Engineering based model level ice & ridged ice included taken from (Kotovirta et al., 2009)	Ice model HELMI	Ship operations & route optimization for the Baltic Sea
Schütz, 2014	Stochastic dynamic programming	N/S	Engineering based model, level ice & ridged ice included, taken from (Kotovirta et al., 2009)	N/S	Ship operations & route optimization for the Baltic Sea
2015, Choi et al.	A*	20 × 20 NM, 1 month	Factors multiplied design speed for ridged ice for ridged ice	Ice model	Strategic planning & route optimization for the Arctic Sea
2015, Reimer, 2016, Kaleschke et l.	N/S	2.7 × 2.7 NM, 0.25 h	Model test and campaigns for icebreaker and ice-going ship,level ice & ridged ice	Ice model	Ship operations & route optimization for the Norwegian Sea
2016, Liu et al.	A*	> 10 × 10 NM, 1 day	Ice numerals, no-go areas for a ship, no speed info	Ice egg from Canadian Ice Service	Strategic planning & route optimization for the Canadian Arctic
2017, Piehl et al.	Potential theory via finite element method	N/S, N/A	N/S	N/S	Concept for route optimization for the Baltic Sea
This work	A*	1 × 1 NM, 6 h	Engineering based model, level ice & ridged ice included, adopted from (Kuuliala et al., 2017)	Ice model HELMI	Multi-objective ship operations & route optimization with deviation costs for the Baltic Sea

et al., 2018). The hybrid model as discussed in (Montewka et al., 2018, 2019) consists of switching the speed function that maps ice conditions into operational speed between an engineering-based model based on rigorous ship-ice interaction and a data-driven model based on AIS ship data. The switch is done if the ice concentration goes under a manually given threshold value. One limitation of this approach is that it does not differentiate between shipping routes, where other ships are probably present, and other areas where finding other ships is improbable. Here, in contrast, we construct a mean-field approach that accounts for this feature.

2.2. Ship routing in ice

There are numerous routing methods for ships navigating under weather conditions in open waters, for a recent literature review see for example (Krata and Szlapczynska, 2018). In these methods, numerous objectives are considered, where the most relevant are ship safety, travel time and fuel consumption. Also various modeling techniques are applied. However, for ships navigating in ice-covered waters, fewer solutions offering ice routing exist. One way to group the existing tools is by the type of their ship performance model. It is either a) engineering-based, b) data driven, or c) based on expertise.

The engineering-based models focus on the physics of the ice-breaking process, where the forces due to ship-ice interactions are determined and the resulting added resistance is calculated. The added resistance is used to determine the attainable speed in given ice conditions, see for example (Kotovirta et al., 2009; Frederking, 2003; Piehl et al., 2017). The models of this type can derive the local speed variation of the ship if the local variation of ice conditions is known in sufficient detail. This is called here micro scale ice navigation. When such a micro scale model is aggregated within a macro-scale, i.e. sea scale, ice navigation framework these models can provide information about ship performance including its speed in modeled ice conditions. The accuracy of the macro scale model is then dictated not only by its micro scale counterpart, but also by the resolution of the discrete numerical ice data, as the ice parameters pertaining to a grid cell are assumed to be grid cell averages. Typically, the resolution of the ice data is 1 NM or coarser. The ship speed in a grid cell is then assumed to be the average value related to the average ice parameters.

Data-driven models take advantage of full-scale campaigns for a given ship navigating in ice, where the performance data (ship speed) and ice conditions are recorded and the relation between those two are found. Such a method is accurate for the specific ship within the range of recorded ice conditions, where various ice formations are encountered. However not all features can be recorded and their effect on ship speed properly established, e.g. ice compression. Hence, these models can be considered as appropriate for macro-scale of ice navigation, suitable best for estimation of ship speed and conditions where the ship can get beset in ice, see for example (Kaleschke et al., 2016; Reimer, 2015).

The third group of models, based on experts' judgment tends to describe the joint effect of numerous ice features and operational conditions on the ship safety and sometimes the ship speed. Thus the presence of various formation of first- and multi-year ice is included, as is the presence of icebreakers. These models suit best for the evaluation of safety of ice navigation prior to setting a ship to the seas, while the speed estimation is of secondary requirements expected from those models (Stoddard et al., 2016; Liu et al., 2016).

Another important grouping criterion for the routing tools is their purpose. This specifically relates to whether the tool will be used quantitatively for route finding at operational or strategic level, or qualitatively for safety assessment. Various geographical scales are used to demonstrate the feasibility of developed solutions, varying from very local applications or concepts on a small scale, (Takagi et al., 2014; Piehl et al., 2017), through medium-scale solutions within the Baltic Sea or the Norwegian Sea, (Kotovirta et al., 2009; Reimer, 2015;

Kaleschke et al., 2016) to large-scale solutions attempting to cover the whole Arctic Sea (Nam et al., 2013; Choi et al., 2015; Liu et al., 2016; Frederking, 2003).

Finally, the tools can be grouped by a mathematical approach adopted to route finding problem, as follows: genetic algorithms (Choi et al., 2013), finite element method-based potential theory (Piehl et al., 2017), graph search-based algorithms (Nam et al., 2013; Choi et al., 2015; Guinness et al., 2014; Liu et al., 2016), conjugate direction methods (Kotovirta et al., 2009), stochastic dynamic programming (Schütz, 2014), and probabilistic road map method (Takagi et al., 2014).

The summary of available solutions for ice routing is presented in chronological order in Table 1. There are two main shortcomings in the existing solutions. The first is the accuracy of the model for the ice field where the ship is navigating. The second is the reliability and the appropriateness of the model for ship performance in ice adopted in the routing solution. Considering the first issue, the limiting factor for a given routing task typically is the inadequate spatial and temporal resolution of the available ice information. The application determines the resolution of ice data that should be used. For long term strategic planning of winter navigation or high-level safety assessment for a given sea area, coarse resolution of several miles in space and one or several days in time suffices, see for example (Choi et al., 2015, 2013; Liu et al., 2016; Frederking, 2003). However, for short-term operational planning, namely finding best route through the ice for a given ship, a finer resolution is needed both spatially and temporally as discussed in (Aksenov et al., 2017). Acknowledging the complexity and dynamics of ice cover, the spatial resolution of one nautical mile or below is needed, and the ice information should be refreshed every few hours, rather than days (Berglund et al., 2007).

Considering the second issue, all relevant features affecting the ship speed should be reflected in prospective route optimization tool (Aksenov et al., 2017; Kotovirta et al., 2009). Due to ice motion, level ice is not the most dominant form of ice at sea. Instead the ridged ice, rafted ice and ice compression create difficulties for ice-bound ships (Mussells et al., 2017). On the other hand, the presence of ice channels and availability of ice breakers significantly facilitate the winter navigation. Therefore, these factors should be included in the ship performance model, to ensure that the performance of a ship in given ice conditions and operational context is properly modeled, see (Kotovirta et al., 2009; Montewka et al., 2019).

Pathfinding algorithms, i.e. route searches in graphs, can be divided into multiple categories (Deo and Pang, 1984; Madkour et al., 2017). For instance, those that use heuristics, those that use incremental searches, and those that use neither or both of these. For route finding in ice conditions, simple geometrical heuristics have been previously used to speed up the optimal route finding, e.g. the works using A* in Table 1. For A* to be guaranteed to find the shortest path, its heuristic function must never overestimate the cost of reaching the goal. Hence, the conventional choice is to use the Euclidian distance from the current location to the end point. This optimizes the time to find the optimal path, but degrades the (visual) information value of our integrated time map, which is explained in section 3.7. Hence, we shall here implement A* but employ a trivial heuristic, $h = 0$, which is equivalent to using the Dijsktra pathfinding algorithm.

3. Method

The proposed method consists of a framework that can incorporate multiple objectives in a singular pathfinding problem, shown in Fig. 1, and of the actual pathfinding algorithm that originates from graph theory (Deo and Pang, 1984). The objectives used here are the following: thick and concentrated ice is avoided in favor of thinner ice or no ice to gain faster steaming speed (Section 3.2), ship besetting in ice is avoided in favor to safer routing options (Section 3.2), ice channels are favored when they provide improved speed even when this requires conforming to the speed of convoys navigating in the channels (Section 3.4), and ship grounding is absolutely avoided (Section 3.3). Other objectives may also be added, as shown in Fig. 3, and discussed later in Section 6.

3.1. Multi-objective optimization using probability masks and mapping functions

The routing optimization is ultimately done by minimizing the travel time used by the ship. The general idea to this end is that we computationally reduce the ship speed in hazardous areas to make those areas less attractive with respect to pathfinding. Since the speed varies with respect to the local ice conditions, it is represented with a so-called *speed map*, which is a spatially discretized representation of the ship speed. Specifically, the speed map is a 2D grid, and inside a grid cell the speed is taken as constant. Since the system is time-dependent, i.e. at least the ice situation data changes every 6 h, each discrete time step adds its own speed map.

The proposed framework can incorporate multiple objectives through alterations of these speed maps. In order to do so, each objective is associated with a probability mask and a mapping function that describes the effect of the mask on the speed map. A trivial probability mask would state that its mapping function is valid everywhere (or nowhere), and a binary probability mask would state that the mapping function either is valid or is not valid for a grid cell. Intuitively, the bathymetry information yields a binary probability mask reflecting which grid cells are navigable and in which grid cells the ship would run aground. In Section 3.3, we show how to modify this mask to exclude narrow waterways from the routing search. The ice information obtained from HELMI model (explained in Section 3.2) is determined in a certain area of the Baltic sea, i.e. above 56.74deg latitude, so the binary probability mask is defined accordingly.

3.2. From ice data and ship performance into a speed map

Ice is modeled with the HELMI continuum model that uses 27 different variables (Haapala et al., 2005), and ice data of this form is obtained from the Finnish Meteorological Institute. Of these 27 variables, we consider the 8 most essential ones

$$(\widetilde{C}, \widetilde{h}, \widetilde{C}_L, \widetilde{h}_L, \widetilde{C}_f, \widetilde{h}_f, \widetilde{C}_R, \widetilde{h}_R).$$

These are the concentration $\widetilde{C}$ and the thickness $\widetilde{h}$ for the ice on average, and these two for level, rafted, and ridged ice, respectively. Notation-wise, we mark these parameters with tildes to distinguish them from the ice parameters used in the proposed method. In the following, the 8 variables are transformed into 2 so that first all the other ice except ridged ice is approximated as level ice, and then we present a percolation argument to simplify the concentration representation. These steps are done in order to use the results of (Kuuliala et al., 2017) to map the ship performance in varying ice conditions into speeds and stuck probabilities, which are then integrated to form a speed map.

Level and ridged ice thicknesses h_L and h_R are obtained from

$$h_L = \frac{\widetilde{h}\widetilde{C} - \widetilde{h}_R\widetilde{C}_R}{\widetilde{C}_L} \tag{1}$$

$$h_R = \widetilde{h}_R. \tag{2}$$

Level ice is important in determining the friction, and ridged ice in determining the probabilities of the vessel becoming beset in ice (Fu et al., 2016; Kuuliala et al., 2017). Besetting typically means that when a ship attempts to surpass ridged ice, there is a chance that it is stuck on top of the ridge keel, i.e. underwater ice, meaning that it cannot steam forward nor reverse. Eq. 1 is similar to previous approaches. In (Kotovirta et al., 2009, see Eq. (18) there-in) h_R is obtained by

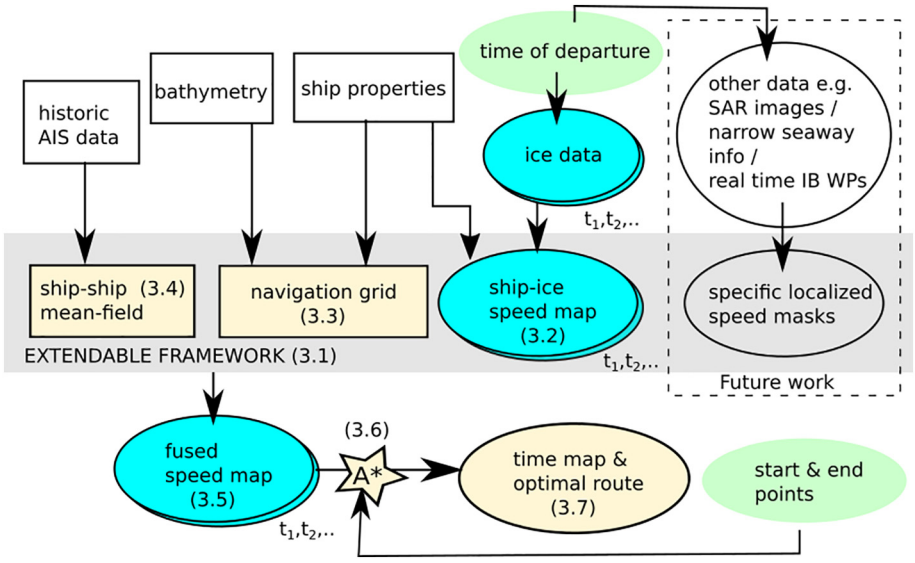

Fig. 1. The proposed method for multi-objective route optimization, implemented as ICEPATHFINDER. Modules are explained in sections indicated by the numbers in parenthesis. The green ellipses represent the manual input necessary to be done on ship. Ellipses are time-dependent information (hourly to daily basis). Boxes contain info that should be updated more rarely, e.g. on a yearly schedule. Ice data and speed maps (cyan) have time steps. Yellow items include new contributions by this paper. (For interpretation of the references to colour in this figure legend, the reader is referred to the web version of this article.)

subtracting h_L from h, and in (Kuuliala et al., 2017, see Eq. (18) therein), equivalent thickness of ridged ice is obtained from HELMI model, and rafted ice thickness is incorporated into level ice thickness.

Ice concentration is a macro-scale statistical measure of how much of the sea surface is covered in ice. When close to zero, the ship is able to find an open water path among the ice. When close to one, there are no options but to ram the ice. In between, there exists a statistical ice concentration threshold above which no continuous open water paths exist. This is known as the percolation threshold, and for a 2D continuum model (assuming that ice lofts are circular) it has a value of $c_{th} = 0.676$ (Rosso, 1989). So, statistically, when the ice concentration is less than c_{th}, the ship can find an open water route, and when above it – it has to go through the ice as modeled in (Kuuliala et al., 2017). Specifically, this affects the total ice concentration

$$C = \begin{cases} \widetilde{C}, & \text{if } \widetilde{C} \geq c_{th} \\ 0, & \text{otherwise} \end{cases}, \tag{3}$$

and the ridged ice concentration

$$C_R = \begin{cases} \widetilde{C}_R, & \text{if } \widetilde{C} \geq c_{th} \\ 0, & \text{otherwise} \end{cases}, \tag{4}$$

where $\widetilde{C}$ and $\widetilde{C}_R$ are the total concentration and the ridged ice concentration obtained from the HELMI model, and C and C_R are the total and ridged ice concentrations used for our model. Note that here the ice ridges are modeled statistically at 1 NM × 1 NM resolution, and that our c_{th} is close to the numerical value of 0.7 that has been used without explanations for similar purposes in (Kotovirta et al., 2009).

Using Eqs. (1), (2), (3), and (4), we write an effective level ice thickness h_i and an equivalent ice thickness h_{eq} as

$$h_i = h_L C \tag{5}$$

$$h_{eq} = h_R C_R \tag{6}$$

The speed in ice-covered waters $\tilde{v}$ and the probability for the ship besetting in ice $\tilde{p}$ are then obtained as

$$\begin{aligned} \tilde{v} &= \tilde{v}(h_{eq}, h_i) \\ \tilde{p} &= \tilde{p}(h_{eq}, h_i) \end{aligned} \tag{7}$$

using a numerical matrix for the mapping from (Kuuliala et al., 2017) results. This matrix is provided within the source code files of ICEPATHFINDER, and is visualized in Fig. 2.

We convert the stuck probability $\tilde{p}$ from Eq. (7) into a delay which penalizes the speed value. Specifically, considering a simple binary pass test with a virtual amount of retries, $N_v \in N$, we write

$$\begin{aligned} v &= \tilde{v}/N_v \\ N_v &\simeq \left(\frac{\log(1 - c_v)}{\log(\tilde{p})} \right), \end{aligned} \tag{8}$$

where the confidence value for passing $c_v = 0.95$, and $\tilde{v}$ and $\tilde{p}$ are obtained from Eq. (7). Note that $v \leq \tilde{v}$, since $N_v \in N$ is enforced. In principle, N_v in Eq. (8) states the equivalent amount of time units that the ship should use to scout a route with no risk. Note that this is a theoretical lower bound estimate, as in practice there is always a risk, and consequently the time is always longer. Computationally, Eq. (8) encapsulates the ice-ship interaction into a single real space value, $v \in R$, which is important because we want to employ unambiguous inequality operators between grid cells to do pathfinding (Section 3.6). Note that although v in Eq. (8) is in fact a *meta-speed* when $\tilde{p} > 0$, we drop the prefix for simplicity.

The speed $v \in R$ of Eq. (8) refers to the speed of the ship in a grid point (i,j) on a given time step t. The speed map $\mathbf{V}_t$ is hence obtained as

$$\mathbf{V}_t = \begin{bmatrix} v_{1,1} & v_{1,2} & \cdots & v_{1,N_S} \\ v_{2,1} & v_{2,2} & \cdots & v_{2,N_S} \\ \vdots & \vdots & \vdots & \vdots \\ v_{M_S,1} & v_{M_S,2} & \cdots & v_{M_S,N_S} \end{bmatrix}, \tag{9}$$

where each grid point is represented by a single scalar speed value obtained from Eq. (8). Speed values near and under 4 knots are treated as zones where independent navigation may be hampered, and ice breaker assistance is mandatory, as shown in the analysis of ship transit (Montewka et al., 2015; Kuuliala et al., 2017). This is expressed with red colour in the speed maps shown in Results (Section 5).

The computational two-dimensional (2D) grid size of $\mathbf{V}_t$ is 1645 × 1113 cells ($M_S \times N_S$). The grid resolution 0.5 × 0.25 NM (nautical mile) follows from the 30-arc-second resolution of GEBCO[1] depth data. At 60 degree latitude, the data is twice as dense longitude-wise than altitude-wise. Although the HELMI data resolution is lower, only 1 × 1 NM, the resolution is kept at GEBCO density to show that a larger grid can be computed in case the ice data resolution increases in the future, or if a larger area of the Arctic is to be modeled.

The ice forecast window of the Finnish Meteorological Institute is two days, with forecasts provided every 6 h. A 2D speed map $\mathbf{V}_t$ is calculated for each time step, and we use 8 time steps $t = 1, 2, \ldots 8$. During this time, it is feasible to navigate from the north end of Gulf of

[1] https://www.gebco.net/

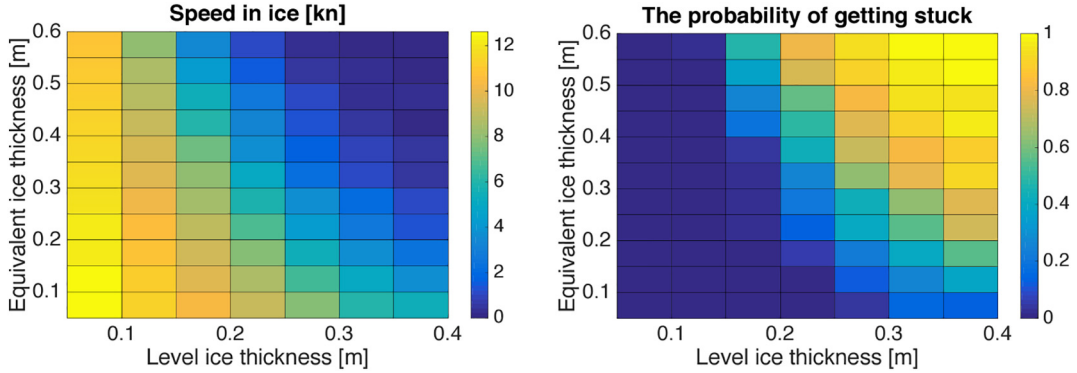

Fig. 2. Visualization of numerical matrices for $\tilde{v}$ and $\tilde{p}$ of Eq. (7) for a specific IA Super class ship, reproduced from (Montewka et al., 2019). The data itself is from the results of (Kuuliala et al., 2017).

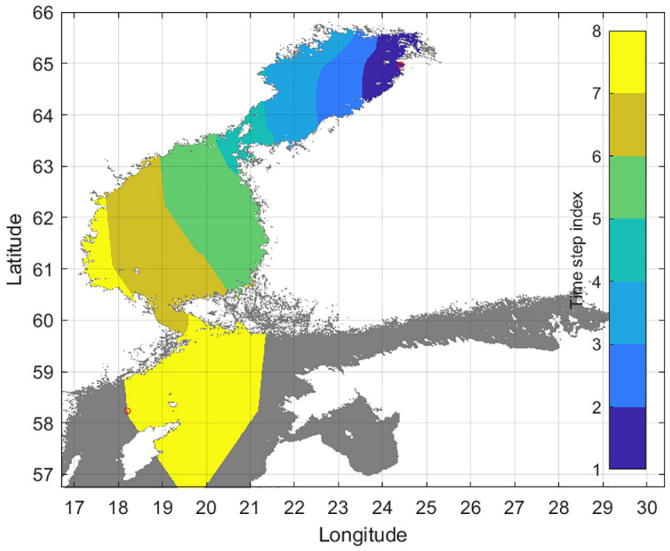

Fig. 3. Computed time step indices for speed maps for a ship traveling from Oulu to near Gotland, $t = 1, 2, ...8$. The time step index is changed for every 6 h of travel time. The propagation speed depends on the ice conditions.

Bothnia, which is normally frozen, to latitude levels near Gotland, where the sea is open all year around. The eight speed maps are given as inputs to the pathfinding algorithm introduced later in Section 3.6. As the path finding algorithm propagates forward in time, the time step (and the speed map) is changed each 6 h of the simulated traveling time, see Fig. 3. This is discussed in more detail in Sections 3.6 and 3.7.

3.3. Narrow waterways in archipelago

Since this is the first study that accesses large sea areas with archipelago, narrow waterways need to be discussed. The resolution of the GEBCO depth map is not sufficient for piloting in narrow waterways, see Fig. 4. Furthermore, the depth map lacks the information of waterways that have been predesignated by authorities as those that should be, or must be, followed, see an example waterway displayed in Fig. 4. In fact, the depth map appears to have unnavigable cells blocking the official waterway with a guaranteed 10 m depth. In other words, the situational awareness obtained for *navigation* purposes is not sufficient for *piloting* purposes. Hence, we need to exclude such areas that are beyond the resolution of our e-Navigation system data.

Computationally, two things are necessary. First, the route start and end points are chosen at the locations where the need for piloting begins. Second, the archipelago needs to be excluded from the speed map so that routes do not run through it. This can be achieved manually by restricting areas within certain latitude and longitude coordinates (i.e. geo-fencing), or autonomously by using dilation operations from image morphology (see e.g. Serra, 1983). We use the latter to effectively rule out all narrow waterways from the GEBCO depth map, also those in archipelagos, having a width of 1 nautical mile or less. See Appendix A for details.

3.4. Ship-ship interaction via a mean-field

Ship navigation is influenced by other ships. This may cause a ship to change its power setting and speed, or to change its course. For example, multiple ships may encounter or follow each other in an ice channel when traversing an ice covered sea area. A model that focuses on the travel of a single ship can be extended to account for multiple ships by introducing a *mean field* with which that single ship interacts. The mean field is constructed from historic AIS data (automatic identification system), see Fig. 5, using a mapping function v_{ch} and a mean field mask M_s. The mapping function is determined from the group speed of interacting ships, see e.g. (Goerlandt et al., 2017a, 2017b) on ship escorts. The mean field mask M_s, on the other hand, is founded on the concept of proximity of one ship to another.

3.4.1. Ship to ship proximity

Proximity, in general, involves not only the distance between the ships but also closeness in time. These two are interconnected by the ship crew's actions in reacting to different navigational situations. With this in mind, we filter the AIS data with a spatio-temporal proximity. Here, proximity is a binary descriptor for identifying situations where a ship's navigation is potentially affected by the presence of another ship. It is used to filter out a subset of AIS data for further analysis of ship-ship interactions. Hence, given a set S of AIS messages an adjacency matrix A of size $N \times N$ is generated, where N is the number of AIS messages in S. The elements of A have value 1 if the proximity condition is met, otherwise they have value 0. Unless this condition is very liberal, the matrix A has a computationally tractable number of non-zeros even for comprehensive sets of daily full update rate AIS for which the message interval is about 10 s for each broadcasting ship ($N \sim 10^7$ messages).

The filter for generating the adjacency matrix A is constructed as follows. An AIS dataset S consists from sets S_j of messages broadcasted by different ships j, formally

$$S = \cup_j S_j.$$

The spatio-temporal data (x, y, t) in S is first discretized with the resolution $(\Delta x, \Delta y, \Delta t)$, and an empty 3D matrix M with the same resolution is created to cover the sea area determined by the overall spatio-temporal ranges of S. For each ship, the discretized data S_j is mapped into elements M_j of the matrix M. The value of an element in M

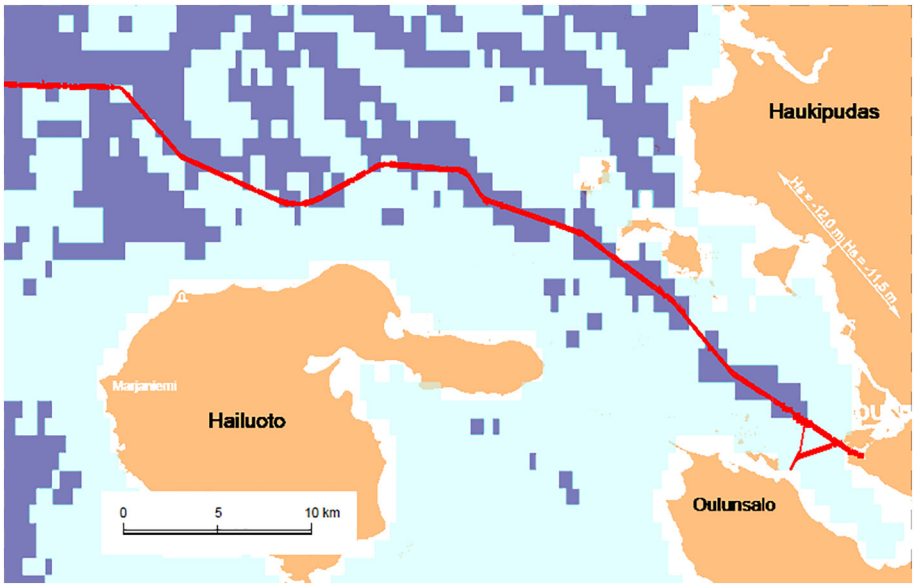

Fig. 4. Example of a narrow waterway. We have plotted the rectangular GEBCO depth grid on top of the map from Finnish Transport Agency showing in red the 10-m-deep waterway to Oulu harbor. We have removed most of the map markings for visual clarity. Navigable depth is shown with dark blue (over 10 m depth) and unnavigable depth is shown with cyan (less than 10 m depth) and white (positive elevation). The waterway width is about 0.5 NM, ≈0.92 km, and piloting services are typically mandatory. (For interpretation of the references to colour in this figure legend, the reader is referred to the web version of this article.)

is increased by j if there is a message in S_j broadcasted from the corresponding discretized spatio-temporal location. When another ship S_k is added, an element of the sum matrix $M = M_j + M_k$ has either the value 0, j, k or $j + k$. The two ships are determined adjacent where an element has the value $j + k$ in M, and they are also adjacent in cases where any two elements with values j and k fit into submatrix W of dimensions $(L_x \times L_y \times L_t)$. This information is then updated into the adjacency matrix A, over all ship pairs. Thus, each element in A either has the value of 0 or 1.

The resolution and the dimensions of W can be chosen to fit the navigational situation at interest. We use the resolution values that have been standard in previous proximity analyses of Baltic winter navigation, see (Lensu and Goerlandt, 2019), $(\Delta°N, \Delta°E, t(hrs)) = (1/60, 1/30, 1/12)$, where the spatial resolution is close to 1 NM at 60°N, and the dimensions of the submatrix W are $(L_x \times L_y \times L_t) = (3 \times 3 \times 2)$. For this choice, all pairs of messages in S_j and S_k are adjacent if their distance is less than 2 NM and time difference less than 5 minutes, and non-adjacent if their distance exceeds $3\sqrt{2}$ NM or their time difference exceeds 10 minutes. Between these all-inclusive and all-exclusive limits the adjacency is fuzzy. The fuzzy margin, which follows from the discretization, can be reduced by increasing the resolution and the size of the submatrix W with the same ratio. The fuzziness can also be removed by calculating true distances and time differences, but this increases computational cost. In the present context of constructing the mean field mask, the standard discrete filtering is considered sufficient as refinements are unlikely to change the mask significantly.

3.4.2. Mean field from ship adjacency

We use the adjacency matrix A to construct a mean field representation for the ship-ship interaction. A ship is either navigating independently in the strict sense, i.e. it has no ship to ship proximity as defined by A, or its navigation is *non-independent*. From this definition we derive two quantities, *the degree of non-independency* and *the intensity of proximity*. In a grid cell (x,y) the degree of non-independency is the ratio of non-independent navigations to all navigations, quantified in terms of the number of AIS messages broadcasted from the cell. The intensity of the proximity in turn is quantified as the average daily number of non-independent navigations. The 1 NM grid of HELMI ice model was used and the result was re-sampled to the grid of the pathfinding algorithm. The intensity of proximity is calculated for icebreakers as the convoy operations are assumed to dominate the mean field. For the mean field, both quantities are calculated as averages over the midwinter period from February to March 2011. The obtained binary mask M_s determines cells inside which independent navigation is not assumed to be an option but all traffic must conform to a system speed v_{ch}.

From Fig. 5 (a) and (b) it is seen that independent navigation is but an exception in certain areas that have either high density of icebreaker operations, difficult ice conditions, or both. The ice conditions shown in Fig. 8 (a) are typical for the period which was characterized by increasing difficulty towards north and east. In the central Bay of Bothnia there are also areas not visited by any ships during the considered period and the traffic mostly follows the principal channels kept open by icebreakers. This is not due to regulations but rather is a common practice.

We use the intensity of proximity for icebreakers, Fig. 5 (b), to initially screen the mean field by requiring that this number exceeds 6 (the bright yellow). This numeral can be much higher in the channel areas but the scale of Figure has been limited in order to make the initial mask better discernible. The mean field mask is then constructed from this by dilation, detection of connected sets, and deleting of isolated cell groups. Within the mask the average speed of all traffic settles to about $8 - 9$ knots when ice thickness exceeds 30 cm, see Fig. 6. This system speed is set by the icebreaker convoys. Therefore, we employ a conservative value of

$$v_{ch} = 8.0 \quad \text{(knots)} \tag{10}$$

in our route calculations. For thinner ice, the higher velocities in Fig. 6 are likely to be due, not only by easier conditions but the possibility of taking over the convoys outside the main channel. In Fig. 6 calculation, the ice thickness is the dominant level ice thickness at the same location where the ship speed is recorded. Thicknesses are obtained from the daily ice maps and are based mainly on observations made from icebreakers.

3.5. Fused speed map from multi-source data

The fused speed maps $\{\mathbf{S}_t\}$ for each time step t are obtained by merging the previous data, namely the ship-ice speed maps $\{\mathbf{V}_t\}$ for each time step t, and the time-independent bathymetry mask R and the ship-ship interaction mask M_s. For each cell $x = (i,j)$,

$$\mathbf{S}_t(\mathbf{x}) = \begin{cases} \mathbf{V}_t(x), & \text{or} \\ v_{ch}, & \text{if} \quad x \in \mathbf{M}_s \quad \text{and} \quad \mathbf{V}_t(\mathbf{x}) < v_{ch} \end{cases} \tag{11}$$

where v_{ch} comes from Eq. (10) and is an estimate for the convoy

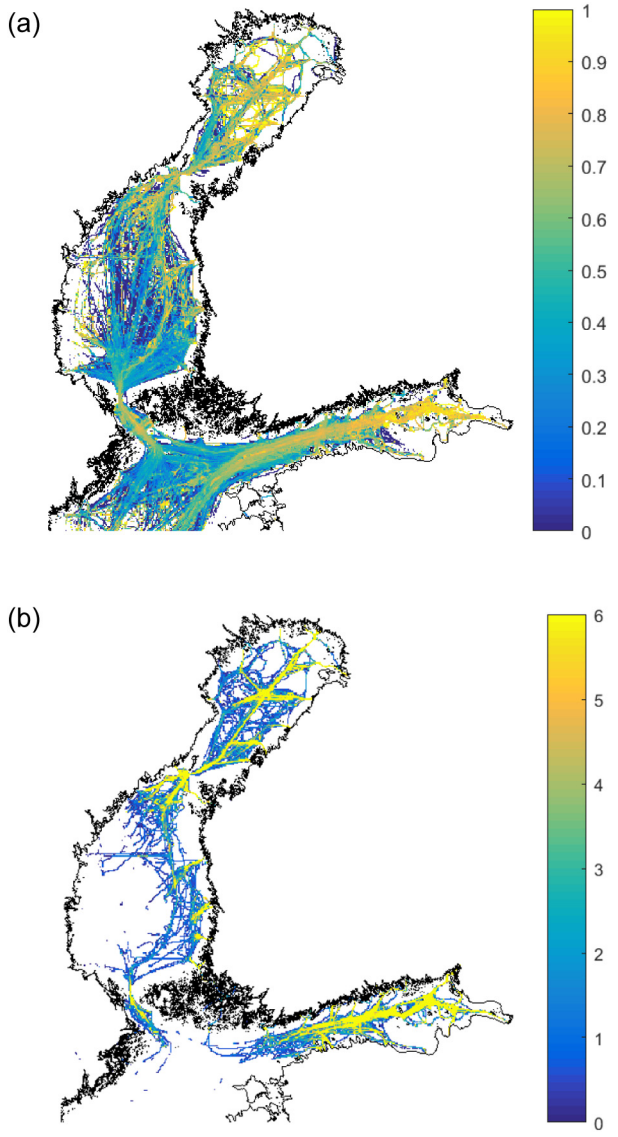

Fig. 5. (a) Degree of non-independent navigation for all ships and (b) the intensity of proximity for icebreaker traffic, both from AIS data for February–March 2011 (see text for explanations).

cruising speed in an ice channel. The bathymetry mask R is employed during the pathfinding to exclude all routes that would overlap with restricted grid cells.

3.6. Pathfinding

For finding the optimal path, our A* algorithm is run on the inverse of the speed map $\mathbf{S}_t$ of Eq. (11), the inverse representing the travel costs in time. A neighborhood of 8 points is used, thus including diagonal directions in the 2D square grid. Formally, the path cost is written as

$$f(n) = g(n) + h(n), \tag{12}$$

where n is the last point on the path, and $g(n)$ is the total cost of traversing from the first point to the point n. Trivial heuristics, $h = 0$, are used to evaluate route deviation costs, which is explained later in Section 3.7. The run is started from the given point A, and stopped when the given end point B is found. If the cumulative time spent on the journey on S_t exceeds the time step difference, the pathfinding continues on the speed next map $\mathbf{S}_{t+1}$, see Fig. 3.

The path P obtained from A* is a series of (diagonally) adjacent grid points

$$P = \{p_1, p_2, p_3, ..., p_N\}. \tag{13}$$

However, such a path obtained from a discretized grid cannot accurately describe the true, geodesically optimal path, see Fig. 7 (a). Nor do ship routes typically contain steep turns, or zigzag motion, which are sometimes included in P.

We relax the dependence of path P on the 2D grid discretization so that it would better represent a ship route, as follows. The method of steepest descent with respect to the path cost (i.e. time) is used to simplify the path, see Fig. 7 (b). Specifically, for each path point p_j, we calculate the change to the total travel time given that that point would be removed

$$\Delta T_j = T(P) - T(P \backslash \{p_j\}). \tag{14}$$

However, if removing a path point would lead to ship grounding, ΔT_j for removing that point equals to negative infinity. The point p_j with the largest positive cost, $\max(T_j) > 0$, is removed yielding a new faster route, $T(P) > T(P \backslash \{p_j\})$. This procedure is repeated until all remaining costs are negative. Hence,

$$T(P) > T(P \backslash \{p_j\}) > T(P \backslash \{p_j, p_k\} > ... > T(P_{wp}). \tag{15}$$

where P_{wp} represents the end result of our iteration, containing a minimum set of way points.

Finally, we compute the geodetic distances between the remaining points P_{wp} of Eq. (15), and obtain steaming times by using interpolated speed values along this path, see Fig. 7 (c). The optimal path is expressed with way-point coordinates, and with speed in knots, time in hours, and distances in nautical miles.

3.7. Time map

Navigation is the art of finding the optimal path. However, computing an optimal path does not per se elaborate any benefits obtained from that path, in contrast to any other available path. Sometimes, two or more paths may be equally good. Therefore, we want to estimate the impact of deviations made from the optimal route, with the help of a so-called (integrated) *time map*. Our time map is obtained by starting the A* algorithm with trivial heuristic, $h = 0$, from both the start and the end points, A and B, and summing up the two travel costs at each grid point. Formally, the total time T calculated for each grid point p_j is

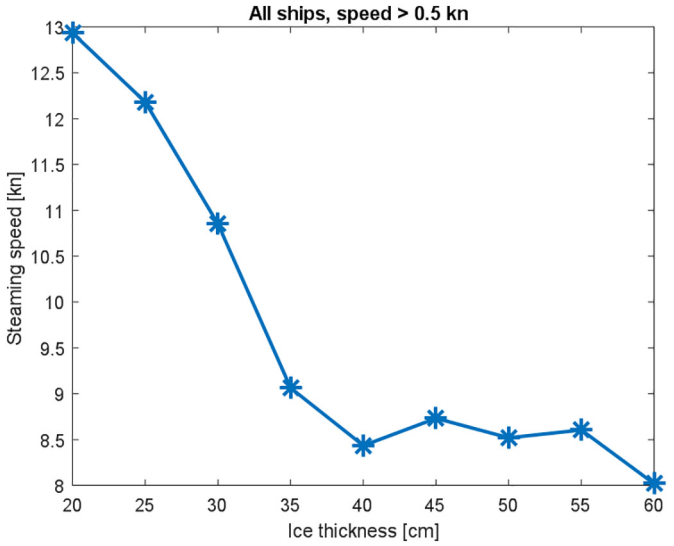

Fig. 6. The steaming speed inside the mean field mask for all traffic during February–March 2011.

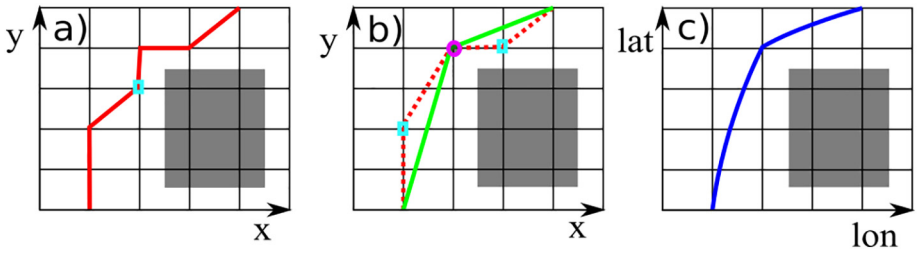

Fig. 7. (a) The optimal route is computed with A* from the speed map $\mathbf{S}_t$, which is a 2D grid. Then the path point whose removal would lead to the largest decrease to the travel time is determined, shown in cyan. The area in grey represents an area that is either unnavigable or has a high traverse cost. (b) The method of steepest descent. The most costly point has been removed leading to the red dotted trajectory. Recursively, further (cyan) points are removed yielding the green trajectory as a result. The removal cost of point surrounded with magenta is negative, so it is not removed. (c) The geodesics are calculated between the optimal path points P_{wp} expressed in latitude and longitude coordinates, forming the fastest route. (For interpretation of the references to colour in this figure legend, the reader is referred to the web version of this article.)

$$T(p_j) = min\left(\int_A^{p_j} v^{-1}(\mathbf{x},\ t)dx + \int_{p_j}^{B} v^{-1}\left(\mathbf{x},\ t\right)dx \right), \tag{16}$$

where the minimum is taken over all the route options, and the speed v is a function of both place x and time t.

Note that the algorithm computes the rightmost term of Eq. (16) actually from B to p_j, instead of from p_j to B. In order to do this, the model time needs to be reversible so that the encountered time-dependent ice conditions are the same regardless of whether the algorithm is propagating forward or backward in time. Therefore, the time stamp at each grid point is saved while propagating forward, and these same time stamps are used while propagating backward, see Fig. 3.

As explained previously, the geometrical sub-cell optimization done after the A star reduces the distance of the shortest path, see Fig. 7. Similar grid topology relaxation and geodesics could be used for each $T(p_j)$ when computing route deviation costs using Eq. (16). However, this would be rather intense computationally and would make sense only in scenarios where different deviation costs need to be expressed with the best available precision. Instead, here we simply scale all times $T(p_j)$ using the ratio between the optimal route time and its non-topology-relaxed grid time, since the time map is intended to be printed out and given as an aid for human eyes.

3.8. Icepathfinder

The source code for the Matlab implementation of the proposed method, called ICEPATHFINDER, is released after publication.[2]

4. Data

Computed routes from and to the named ports are documented in Table 2. The coordinates point not directly to the ports themselves, but to the beginnings of the designated seaways leading to these ports, where pilots need to be employed. These routes are illustrated later in the Results section, see Fig. 9.

Ice data (HELMI) is obtained from FMI so that each time step is represented by a 556 × 415 resolution Matlab data file. We use historical data from February and March of 2011, representing a cold winter. Metaspeed numerical matrix for a certain anonymous ship with the ice class'IA super' is obtained from the authors of (Kuuliala et al., 2017). The ship is a bulk carrier with DWT 21353 tons and a length of 149 m. Bathymetry information is obtained from GEBCO.

For method validation purposes, comparison data is used for Kemi and Hamina routes, as indicated in Table 2. This comparison data consists of historic AIS routes of certain ships that has the same ice class, i.e. IA super, as the ship for which metaspeed matrix is employed, and also of two routes planned by a seasoned arctic seafarer. Prior to a route planning, the seafarer was given the approximate start and end coordinates as in Table 2, the ice map for that specific departure time provided by the FMI (such as the one in Fig. 8 (a)), and regular navigation charts with pencils and compasses. In other words, no computed results or AIS routes were shown or discussed with the seafarer prior to the planning. For elaboration and more results, see (Lehtola et al., 2018).

Table 2
The four computed routes with latitude and longitude coordinates. (*: Comparison data presented.)

From	Lat long	To	Lat long	Date
Oulu	65.159 24.442	Baltic	58.737 19.071	2011-02-03
Kotka	60.200 26.400	Baltic	58.240 19.672	2011-03-01
Kemi*	65.577 24.328	Baltic	58.853 19.409	2011-03-20
Hamina*	60.446 27.264	Rauma	65.082 25.023	2011-03-15

5. Results

When geo-information covering large sea areas can be processed and visualized, the distinctions between regions become visible. In Fig. 8, the ice map provided by weather services is shown alongside the speed map obtained from the proposed method. Note that while the ice map shows a constant red colour for the ridged ice field, which covers the whole east side of the Gulf of Bothnia, the speed map distinguishes the northern part where an ice breaker is needed from the southern part as an area where the ship can operate by itself. This is because the change in concentrations of the different ice types is hard to visualize on the ice map, but not on the speed map. Ice eggs are printed to ice maps to communicate this change in concentrations, but the eggs are also somewhat challenging to interpret.

With the proposed method, routes spanning the whole Baltic area can be evaluated. Using GEBCO bathymetry data directly with ship draught (=10 m) leads to computational routes that run through archipelagos, see the red routes in Fig. 9 (a). As discussed in the Methods subsection 3.3, these areas need to be excluded. This is done by image morphology, leading into three major improvements in routing, visible in Fig. 9 (b). The Archipelago Sea archipelago from the Hamina-Rauma route and the Stockholm archipelago from the Oulu route are correctly excluded, as are the passageways between coastline islands and the continent. The effect of the latter is especially visible near the coasts of central Gulf of Finland. However, this is not sufficient to the most challenging landscapes. In addition, manual geo-fencing is required to restrict passage to regulated piloting-only areas, e.g. navigating south of Naissaari, near Tallinn, or using the North Kvarken passage. The changes imposed by these restrictions are included in Fig. 9 (b), where the new computational routes are shown in black.

We validate our narrow passageway method against AIS data. Specifically, we extract a mask of areas where ships have navigated from the non-independency map of Fig. 5, which contains data of all ships that have visited the Baltic sea above 58deg latitude. The extraction includes filling the mask on open sea areas that are surrounded by ship routes. This all-ships-mask describes which parts of the sea are navigable. The comparison between it and our computationally

[2] https://github.com/vlehtola/icepathfinder

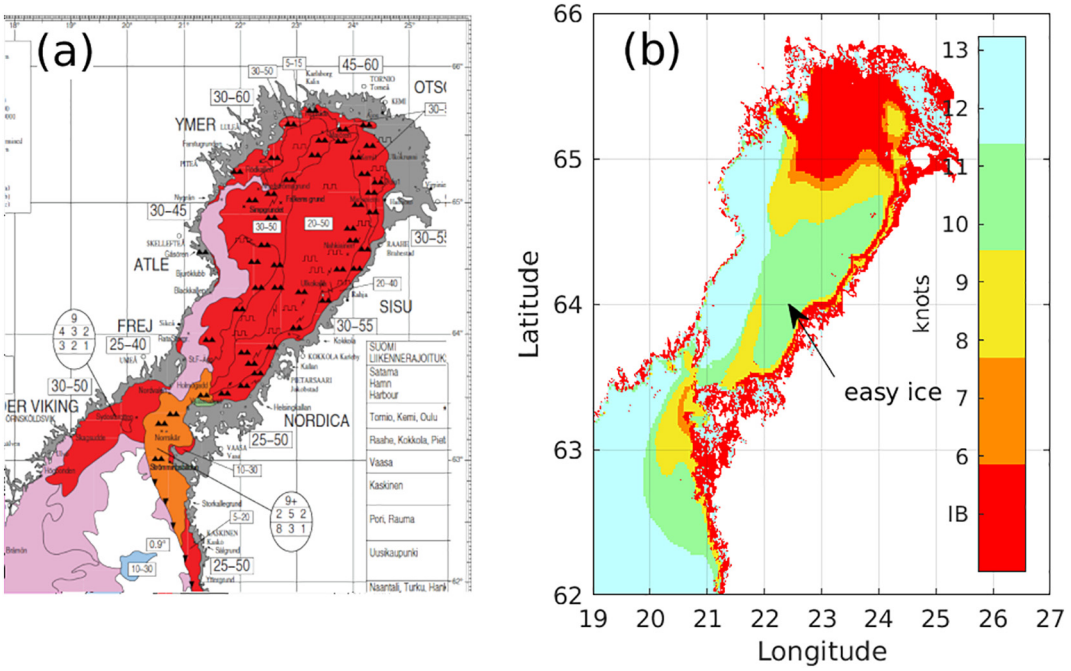

Fig. 8. (a) The ice egg information in the ice map provided currently by Finnish or Swedish authorities is more transiently represented with (b) the speed map of Eq. (9). From the map coloring in (b), the need for an ice breaker is concretely revealed. Legend: ridged ice (▲▲).

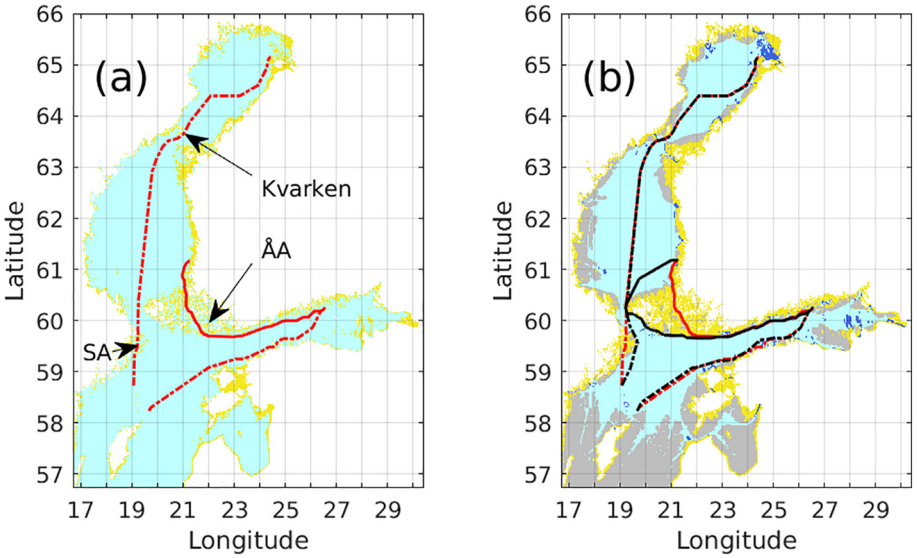

Fig. 9. (a) Unnavigable golden areas are determined from GEBCO bathymetry grid and ship draught. Red computed routes enter archipelagos. ÅA and SA stand for Åland and Stockholm archipelagos, respectively. (b) The proposed method excludes narrow seaways requiring piloting, and new computed routes are plotted in black. The method is validated as follows. Grey areas are navigable in simulations, but have not been visited by ships during the AIS data period. Deep blue areas are not navigable in simulations, but have been visited by ships. The AIS data record is incomplete near 58deg latitude and below. (For interpretation of the references to colour in this figure legend, the reader is referred to the web version of this article.)

morphed bathymetry grid is seen in Fig. 9, with discrepancies shown in grey and deep blue. Deep blue areas have been visited by ships, but are designated as unnavigable in the simulations. Grey areas represent the vice versa. One explanation to the existence of these deep blue areas is that these areas might have been visited by ships with a smaller draught than 10 m, which is the value used in our simulations. Grey areas are partly explained by AIS data record incompleteness, especially near 58deg latitude and below. Considering these explanations, the match between the result from the proposed method and the validation mask is good. In other words, the algorithm is accurate in restricting the areas, where the proposed navigation method is not valid, and accurate in keeping the areas, where it is valid.

Given the start and end points for the journey, and the departure time, the speed maps $\mathbf{S}_t$, the optimal path and an integrated time map can be computed, see Fig. 10 (a) and (b). For human eyes, a time map offers richer geo-information than mere the optimal path, see Fig. 10. In particular, it visualizes the cost for deviating from the optimal route. On the one hand, if the algorithm recommends a detour around some specific area, the time map brings forth the justification behind this. One the other hand, if there are areas with equivalent travel costs, these are similarly visualized. In other words, a time map displays what should be the precision with which to follow the optimal course. It tells the navigator nothing less than — the benefit of following the computed optimal route.

In order to validate our routing method, we look at the historic AIS data of the specific days the travels are simulated, listed in Table 2. AIS data from IA super -ice class ships is selected, i.e., the same ice class than the one for which the metaspeed matrix was obtained, but otherwise ships may be different. A steaming times comparison between these AIS times and the simulated results is shown in Table 3. Because the model ship and the real ship may be different, we normalize the AIS steaming times t_{AIS} for comparison purposes using the

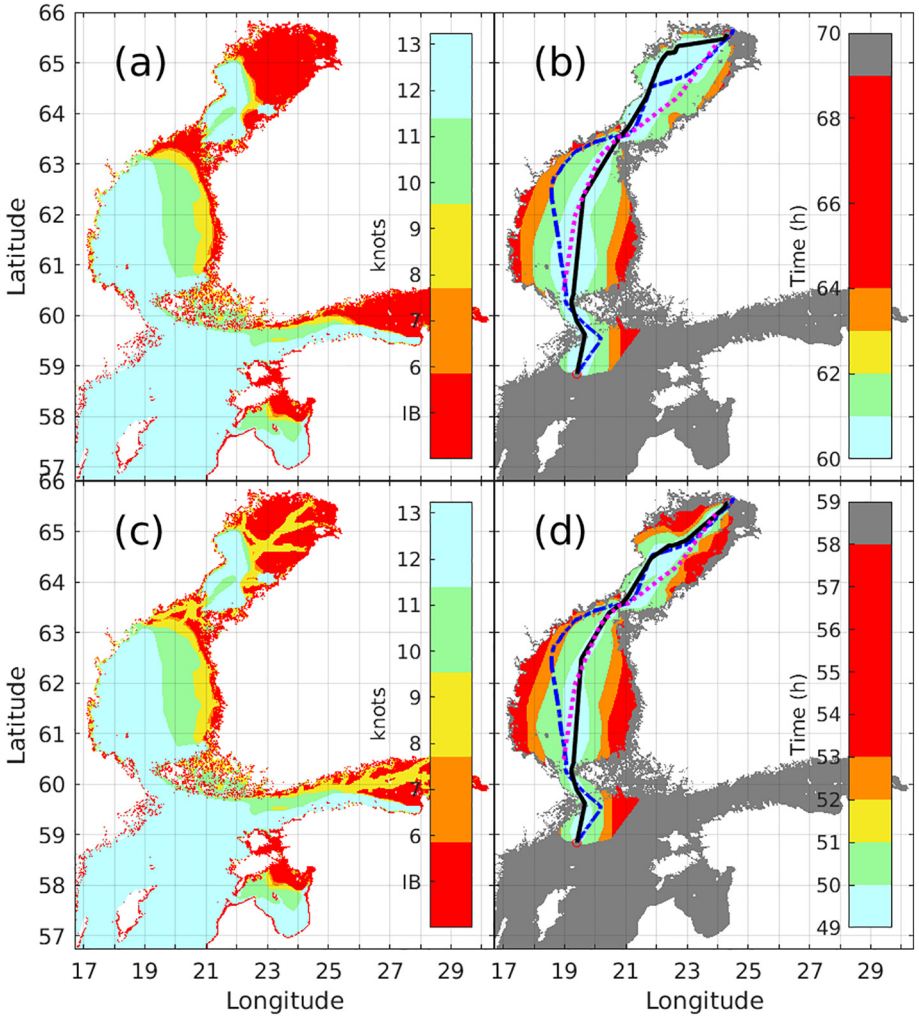

Fig. 10. (a) Speed map of Eq. (9) expressed in knots for the Kemi route. (b) Time map indicating the cost in time when deviating from the optimal (black) route. The slashed blue line is the AIS historic path taken by a similar A1 super -class ship traveling on the given day. The dotted magenta line represents a preliminary route plan by a seafarer seasoned in ice navigation, obtained from a pen and paper exercise given that day's ice map. (c) Fused speed map of Eq. (11) including the ship-ship interaction mean-field. (d) Time map and the optimal (black) route obtained from (c). (For interpretation of the references to colour in this figure legend, the reader is referred to the web version of this article.)

Table 3
Rough steaming times comparison for each route (in hours). AIS times t_{AIS} are from other IA super ice class ships traveling the route on the specific same day. These AIS times are normalized with respect to open water velocities into $\hat{t}_{AIS}$.

Route	Distance (NM)	Simulation (h)	$\hat{t}_{AIS}$ (h)	t_{AIS} (h)
Oulu	487	45.2	49.6	43.4
Hamina	341	18.9	30.3	19.9
Kemi	498	49.1	56.4	42.1
Kotka	307	14.2	18.2	12.5

open water steaming speed of our model ship $v_{top} = 13.2$ knots, and the median value of the speed of the other ship. This normalization should be independent of temporary ice slowdowns, as ice does not affect the open water steaming speed and ships are assumed to steam mostly outside ice-covered regions. Obviously, this comparison is very rough, and should be considered accordingly. The normalized times $\hat{t}_{AIS}$ are shown in Table 3. With the ship-ship interaction mean-field, shown in Fig. 10 (d), the steaming time is 49.1 hours, and without it 59.6 hours, shown in Fig. 10 (b). Note also, how the routes differ. For a significantly longer route, the normalized AIS time is $\hat{t}_{AIS} = 56.4$ hours (see Table 3). This implies that the use of the proposed mean-field brings the results closer to reality, since the ship is typically not alone but follows ice channels in the Gulf of Bothnia. From the comparison in Table 3, the routing is optimized for all routes.

In Fig. 10 (b), the AIS route and the computed path differ in the Gulf of Bothnia and south of Kvarken. The first difference is due to the omittance of the ship-ship interaction, which is introduced in Fig. 10 (d), bringing the two routes close to one another. The second difference is probably due to that that the ice breaker-assigned route, a so-called dirway, has been close to the Swedish coastline during that day. The computed route instead uses a statistical mask for ship-ship interactions.

For further validation, we asked help from a seafarer seasoned in ice navigation, see Section 4. The two routes that were planned are shown with dashed blue lines in Figs. 10 and 11. Note that south of Kvarken the planned route in Fig. 10 (d) is very similar to the one obtained from the proposed method. Hence, we can conclude that the only difference between these two routes and the AIS route is, in fact, the dirway position, which was unknown to both our method and the seafarer. North of Kvarken, on the other hand, the proposed route follows the AIS route. By Fig. 10 (c), this is the route with both least ice and a high probability for assistance.

5.1. Risk of turning winds

The wind has blown from the north creating an ice-free fast line near the coast in the Gulf of Finland, visible from the speed map shown in 11 (a). Hence, in Fig. 11 (b), the optimal route follows that lane near the coast. However, if the wind turns, and does so abruptly, there is a significant risk for a ship besetting in ice when the gap closes. Furthermore, the situation for the ship resembles being between a hammer and an anvil, if the ice closing in was previously ridged. The seafarer-planned route (dashed blue) and the historical AIS route (dotted

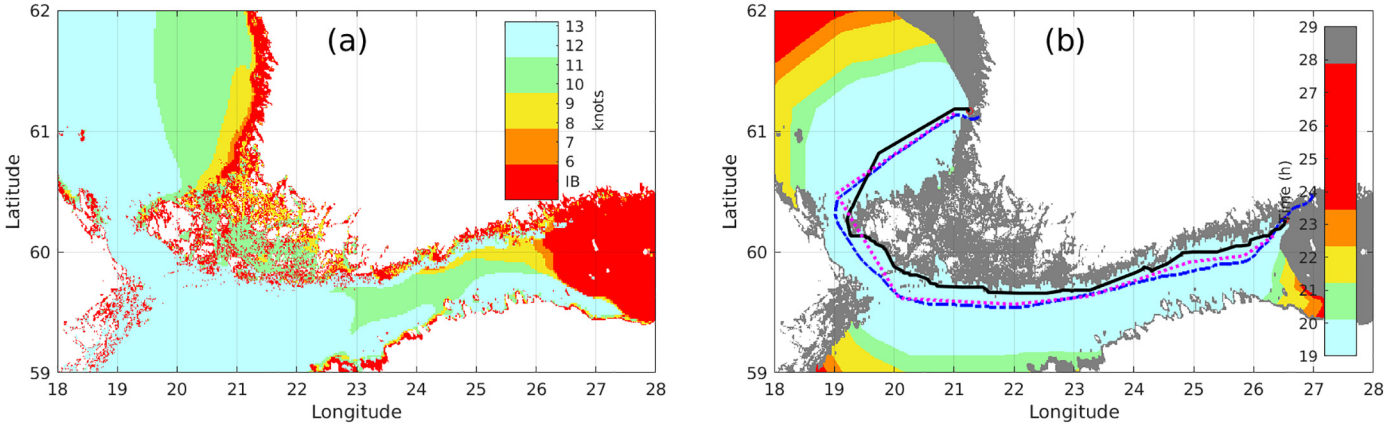

Fig. 11. Risk aversion on the route from Hamina to Rauma. (a) The fused speed map. (b) The time map introduces an estimate for the travel time (in hours), and another for the delays (see colorbar) should the ship follow some other than the computationally optimal path (black line). The optimal path follows the Finnish coastline, the seafarer-planned route (dashed blue) and the historical AIS route (dotted magenta) of a certain ship on the given day take a more conservative approach. (For interpretation of the references to colour in this figure legend, the reader is referred to the web version of this article.)

magenta) of a certain ship on the given day take a more conservative approach, avoiding the possibility that the wind turns, see Fig. 11 (b).

Route optimization is a trade-off between risk and gain. Our model sees no risk of turning wind, even though it uses a 48 h ice prediction forecast. This can be interpreted from the layout of the computed route in Fig. 11 (b). Whether there is a risk, and whether this risk is appropriately modeled boils down to the accuracy of weather prediction, which in turn determines the accuracy of the ice prediction model (HELMI).

5.2. Computational Performance

The computational efficiency of our Matlab implementation, ICEPATHFINDER, is evaluated using the obtained CPU times in minutes with a 2.7 GHz processor, see Table 4. Even the time maps for the longest routes from south to the end of Gulf of Bothnia are computed in less than half an hour. This includes running the dynamic search algorithm (A star) two times to get the time map. The grid resolution of 0.5 NM × 0.25 NM is a lot denser than the HELMI model grid resolution 1 NM × 1 NM, so the computation times are overestimates of what would be actually needed to process current ice data. Optimal routes are obtained in half the time expressed in Table 4, and speed maps S_t in less than a minute.

6. Discussion

The presented speed maps imply that the information about the concentrations of different ice types is important for independent navigation. This information has been previously expressed with ice eggs that, however, are hard to read. Undoubtedly this is the reason why Finnish and Swedish authorities seldom print these ice eggs onto ice maps. The proposed speed map, in contrast, offers the same information as the ice eggs without the sacrifice in visual appearance. This turns a trade-off into a double-benefit scenario. The speed map concretely reveals where the ship specifically needs the aid of an ice breaker.

The safety of the computed routes depends on the accuracy of weather forecasts, especially the direction and strength of winds. If the wind turns and pushes the ice off the coast, the computationally optimal route might be found within this gap. However, if the wind turns again, and does so abruptly, there is a significant risk for a ship in besetting in ice when the gap closes. We describe the situation for the ship to resemble as being between a hammer and an anvil, if the ice closing in was previously ridged. In order to avoid such incidents, and for increasing method reliability, the weather forecasting should aim towards more forecast-friendly, probabilistic models.

Table 4
CPU times in minutes used to obtain (integrated) time maps for each route.

Route	Distance (nm)	CPUtime (min)
Oulu	487	17.1
Hamina	341	19.0
Kemi	498	17.7
Kotka	306	11.8

Apart from inaccuracies in weather prediction forecasts, there are other shortcomings why the speed maps as implemented in the current approach may not be fully accurate representations of the attainable speed in ice conditions. First, the ice maps are discretized in time steps of 6 hours, from which the speed maps are derived. Changing conditions between these time steps are not accounted for. Second, the relation between the ice map data and the vessel speed performance is based on a model presented in (Kuuliala et al., 2017). It is acknowledged that this ship performance model contains several assumptions and uncertainties related to the parameters, which may affect the accuracy of the speed map compared to the actually attainable speed. It is an avenue for future research to validate this model for navigation in other ice-covered waters (e.g. the Arctic), where other ice conditions such as multi-year ice occur. Third, another limitation of the current modeling approach is that the route optimization does not account for the loads incurred by the ship during its passage through the ice fields. Empirical evidence shows that that both ice thickness and ship speed lead to higher ice loads encountered by a vessel (Kotilainen et al., 2017). Thus higher transit speeds in heavier ice conditions might be related to higher probabilities of hull damages and higher related repair costs. The current routing algorithm does not consider these effects. Further research could also include hull damage probabilities as an objective for the routing algorithm. Fourth, more details that are related to the ice model should be accounted for, including ice pressure, resistance from snow, and different stages of ice melting. This especially feasible when the preliminary estimations that exist in e.g. HELMI ice model (Haapala et al., 2005) become more accurate.

Winter navigation in the Baltic Sea has systemic characteristics due to most traffic steaming in a network of ice channels. This affects also ships that would be able to proceed towards a destination without assistance. In thicker ice they must make their choice between slower but more economic steaming in an ice channel and faster but fuel consuming independent transit outside channels which may also involve hull damage and besetting risks. A fully developed route optimization should include not only the present state of the navigation system but time-propagated future projections of that state as well. These could be

provided by land based services which have access to all traffic and environmental data.

In the future, ice models are likely to have a better temporal and spatial resolution, for example, from a better synthesis with Synthetic Aperture Radar (SAR) satellite data. SAR images could provide updates on whereabouts of ice channels, with the update frequency being dependent on the satellite operations. Consequently, this surge towards better temporal and spatial resolution is likely to create a need for incremental pathfinding algorithms such as D* (Stentz, 1994) or D* Lite (Koenig and Likhachev, (2005) that can deal with an information imbalance, i.e. when some areas of the environment (seen by the satellite) are better known than some other areas, or when changing the route is mandatory, for example because of another vessel is stuck in an ice channel, or because a new ice breaker route is introduced during the present journey. Also, multi-ship route planning for traffic control purposes could also be considered.

When moving towards automation, ships are likely to have more sensors on board, which increases their situational awareness. This information, in conjunction with that obtained from other ships of similar kind, could then be fused to further aid the finding of a best possible route (Wróbel et al., 2018). This would mean that the spatial knowledge on ice conditions would be even more inhomogeneous, since better resolution data would be available close to the ships, and from along their past trajectories. In combining this data with the probabilistic ice models of the future, incremental searches such as (Stentz, 1994; Koenig and Likhachev, 2005) would again become useful.

7. Conclusion

Planning safe and efficient routes reduces the risk of a ship besetting in ice, the risk of ship grounding, but also unnecessary delays. Here, we have made four contributions. We presented (1) a generic framework which enables the integration of multi-source data into a set of probability masks and mapping functions, from which time stamped speed maps and, ultimately, the optimal route can be computed. This way, multiple objectives can be accounted for. For example, we employed bathymetry data and image morphology techniques to automatically mark the area where our e-Navigation method is viable. Another major contribution lies in (2) proposing the inclusion of ship-ship interactions statistically with a mean-field model to account for artificial ice channels and ship convoys. This dissolves the discrepancy between the models and reality in independent ice navigation.

Optimal routes are found with (3) the proposed A*-based method, yielding the following outcome: waypoints expressed with geographical coordinates, expected speed and travel time over each route leg, and the estimated time of arrival to destination. Importantly, the output has not only been relaxed with respect to the discretization of the input data, but is also geometrically optimized up to the point where the path consists of geodesics that conform to the shape of the Earth's surface. In addition, running the pathfinding algorithm twice yields (4) an integrated steaming time map, which indicates the cost estimates for deviating from the optimal path. Put more straightforwardly, this time map determines the use value of the computed optimal path.

The proposed method has been validated with both historic AIS data and two routes planned by a seasoned seafarer. Our time map as well as our speed map are 2D grids, which is a rather general format to represent geo-information. This format easily allows for further processing. The reported CPU run times are of magnitude suitable for onboard implementations. Hence, our results imply that the proposed method, including the multi-objective framework and the route finding algorithm, should be quite universally applicable in (automated) maritime navigation.

Acknowledgments

The work in this article has mainly been carried out in the context of the BONUS STORMWINDS project. This project has received funding from BONUS (Art 185) funded jointly from the European Union's Seventh Programme for research, technological development and demonstration, and from the Academy of Finland. In addition, F.G. thanks for funding received from the Ocean Frontier Institute, for the project'Safe Navigation & Environmental Protection'.

Appendix A. Appendix

Consider that the islands and non-navigable depths are expressed as values of one in a binary image B, where the navigable sea is represented by values of zero. We employ a dilation kernel

$$D = \begin{bmatrix} 1 & 1 & 1 \\ 1 & 1 & 1 \\ 1 & 1 & 1 \end{bmatrix} \tag{17}$$

to enlarge the non-navigable area, and obtain

$$R = B \oplus D, \tag{18}$$

where $\oplus$ is the dilation operator (see e.g. Serra, 1983). In R, the narrow waterways in archipelago are enclosed from all sides where there is land or a non-navigable depth. The use of this method requires defining the characteristic width w_c of what is a narrow waterway. The resolution of B should then be half of that, since the enclosing takes place from both sides.

In this work, the GEBCO depth map is used as B in Eq. (18). We first employ one dilation operation with a total span of 2 nautical miles (D is 5×5), and then relax the geometry with one *erosion* operation with a total span of 1 nautical mile (D is 3×3). The dilation operation is necessary to in order to be certain in closing the waterways with an effective width $w_c = 1$ nautical mile, and the erosion operation to prevent ruling out an unnecessary amount of water. Concurrently, the Åland archipelago, the Stockholm archipelago, and the archipelago at the coast of Finland are all excluded. Northern Kvarken route is manually excluded, i.e. geo-fenced, since both the north and south routes are wider than 1 NM, and the North Kvarken route is not typically used by merchant vessels for safety and regulatory reasons (area shown in Fig. 9). Similarly for example the passage south of Naissaari, near Tallinn, needs to be geo-fenced.

References

Aksenov, Y., Popova, E.E., Yool, A., Nurser, A.J.G., Williams, T.D., Bertino, L., Bergh, J., Jan. 2017. On the future navigability of arctic sea routes: high-resolution projections of the arctic ocean and sea ice. Mar. Policy 750 (Supplement C), 300–317.

Barabadi, A., Gudmestad, O.T., Barabady, J., 2015. Rams data collection under arctic conditions. Reliab. Eng. Syst. Saf. 135, 92–99. https://doi.org/10.1016/j.ress.2014.11.008. ISSN 0951-8320.

Berglund, R., Kotovirta, V., SeinÃ, A., 2007. A system for icebreaker navigation and assistance planning using spaceborne sar information in the baltic sea. Can. J. Remote. Sens. 330 (5), 378–387. https://doi.org/10.5589/m07-042.

Beveridge, L., Fournier, M., Lasserre, F., Huang, L., Têtu, P.-L., 2016. Interest of asian shipping companies in navigating the arctic. Polar Sci. 100 (3), 404–414.

Boström, M., Österman, C., 2017. Improving operational safety during icebreaker operations. WMU J. Marit. Aff. 160 (1), 73–88.

Bye, R.J., Aalberg, A.L., 2018. Maritime navigation accidents and risk indicators: An exploratory statistical analysis using ais data and accident reports. Reliab. Eng. Syst. Saf. 176, 174–186. https://doi.org/10.1016/j.ress.2018.03.033. ISSN 0951–8320.

Choi, M., Chung, H., Yamaguchi, H., De Silva, L.W.A., 2013. Application of genetic algorithm to ship route optimization in ice navigation. In: Proceedings of the International Conference on Port and Ocean Engineering under Arctic Conditions. *POAC*. Lulea University of Technology (URL).

Choi, M., Chung, H., Yamaguchi, H., Nagakawa, K., 2015. Arctic sea route path planning based on an uncertain ice prediction model. Cold Reg. Sci. Technol. 109, 61–69. https://doi.org/10.1016/j.coldregions.2014.10.001. ISSN 0165-232X. (URL).

Deo, N., Pang, C.-Y., 1984. Shortest-path algorithms: taxonomy and annotation. Networks 140 (2), 275–323.

Dong, Y., Frangopol, D.M., Sabatino, S., 2016. A decision support system for mission-based ship routing considering multiple performance criteria. Reliab. Eng. Syst. Saf. 150, 190–201. https://doi.org/10.1016/j.ress.2016.02.002. ISSN 0951–8320. (URL).

Erceg, S., Ehlers, S., Jan. 2017. Semi-empirical level ice resistance prediction methods. Ship Technol. Res. 640 (1), 1–14.

R. Frederking. A model for ship routing in ice. In S. Loset, B. Bonnemaire, and M. Bjerkas, Editors, Proceeding of the 17th International Conference on Port andc Ocean Engineering under Arctic Conditions, POAC'03, Trondheim, 2003.

Fu, S., Zhang, D., Montewka, J., Yan, X., Zio, E., Nov. 2016. Towards a probabilistic model for predicting ship besetting in ice in arctic waters. Reliab. Eng. Syst. Saf. 1550 (Supplement C), 124–136.

Ghosh, S., Rubly, C., July 2015. The emergence of arctic shipping: issues, threats, costs, and risk-mitigating strategies of the polar code. Austr. J. Maritime Ocean Affair. 70 (3), 171–182.

Goerlandt, F., Goite, H., Valdez Banda, O.A., Höglund, A., Ahonen-Rainio, P., Lensu, M., 2017a. An analysis of wintertime navigational accidents in the northern Baltic Sea. Saf. Sci. 92, 66–84 Feb. (a).

Goerlandt, F., Montewka, J., Zhang, W., Kujala, P., 2017b. An analysis of ship escort and convoy operations in ice conditions. Saf. Sci. 95, 198–209. https://doi.org/10.1016/j.ssci.2016.01.004. b. ISSN 0925–7535. (URL).

Gong, H., Polojärvi, A., Tuhkuri, J., et al., 2017. Preliminary 3d Dem Simulations on Ridge Keel Resistance on Ships. POAC.

Guinness, R.E., Saarimäki, J., Ruotsalainen, L., Kuusniemi, H., Goerlandt, F., Montewka, J., Berglund, R., Kotovirta, V., May 2014. A method for ice-aware maritime route optimization. In: 2014 IEEE/ION Position, Location and Navigation Symposium - PLANS 2014, pp. 1371–1378.

Haapala, J., Lönnroth, N., Stössel, A., 2005. A numerical study of open water formation in sea ice. J. Geophys. Res. (C9), 1100.

Jalonen, R., Riska, K., Hänninen, S., 2005. A preliminary risk analysis of winter navigation in the Baltic Sea. Finnish Maritime Administration.

Kaleschke, L., Tian-Kunze, X., Maaß, N., Beitsch, A., Wernecke, A., Miernecki, M., Müller, G., Fock, B.H., Gierisch, A.M.U., Heinke Schlünzen, K., Pohlmann, T., Dobrynin, M., Hendricks, S., Asseng, J., Gerdes, R., Jochmann, P., Reimer, N., Holfort, J., Melsheimer, C., Heygster, G., Spreen, G., Gerland, S., King, J., Skou, N., Søbjaerg, S.S., Haas, C., Richter, F., Casal, T., 2016. SMOS Sea ice product: Operational application and validation in the Barents Sea marginal ice zone. Remote Sens. Environ. 180, 264–273. https://doi.org/10.1016/j.rse.2016.03.009. (URL).

A. Keinonen, R. Browne, and C. Revill. Icebreaker design sythesis phase 2. Analysis of Contemporary Icebreaker Performance. Technical report, Transport Canada, TP 10923E, Ottawa, 1991.

Khan, B., Khan, F., Veitch, B., Yang, M., Jan. 2018. An operational risk analysis tool to analyze marine transportation in arctic waters. Reliab. Eng. Syst. Saf. 169, 485–502.

Koenig, S., Likhachev, M., 2005. Fast replanning for navigation in unknown terrain. IEEE Trans. Robot. 210 (3), 354–363.

Kotilainen, M., Vanhatalo, J., Suominen, M., Kujala, P., Mar. 2017. Predicting ice-induced load amplitudes on ship bow conditional on ice thickness and ship speed in the Baltic Sea. Cold Reg. Sci. Technol. 135, 116–126.

Kotovirta, V., Jalonen, R., Axell, L., Riska, K., Berglund, R., Jan. 2009. A system for route optimization in ice-covered waters. Cold Reg. Sci. Technol. 550 (1), 52–62.

Krata, P., Szlapczynska, J., 2018. Ship weather routing optimization with dynamic constraints based on reliable synchronous roll prediction. Ocean Eng. 150, 124–137. https://doi.org/10.1016/j.oceaneng.2017.12.049. ISSN 0029–8018. (URL).

Kubat, I., 2012. Quantifying Ice pressure Conditions and predicting the risk of Ship Besetting. In: *International Conference and Exhibition on Performance of Ships and Structures in Ice 2012 (ICETECH 2012)*. Society of Naval Architects and Marine Engineers (SNAME).

Kum, S., Sahin, B., Apr. 2015. A root cause analysis for arctic marine accidents from 1993 to 2011. Saf. Sci. 740 (Supplement C), 206–220.

Kum, S., Sahin, B., 2016. A Survey on Ice Navigation Research. *Transactions of Navigation*.

Kuuliala, L., Kujala, P., Suominen, M., Montewka, J., Mar. 2017. Estimating operability of ships in ridged ice fields. Cold Reg. Sci. Technol. 1350 (Supplement C), 51–61.

Lasserre, F., Pelletier, S., 2011. Polar super seaways? Maritime transport in the arctic: an analysis of shipownersâ€™ intentions. J. Transp. Geogr. 190 (6), 1465–1473.

Le Boudec, J.-Y., McDonald, D., Mundinger, J., 2007. A generic mean field convergence result for systems of interacting objects. In: *Quantitative Evaluation of Systems, 2007. QEST 2007. Fourth International Conference on the*, pages 3–18, IEEE.

Lehtola, V., Montewka, J., Salokannel, J., 2018. Sea captainsâ€™ Take on Automated Ship Route Optimization in Ice-Covered Waters.

Lensu, M., Goerlandt, F., 2019. Big maritime data for the Baltic Sea with a focus on the winter navigation system. Mar. Policy 104, 53–65.

Lépy, É., Jan. 2013. The recent history of finnish winter navigation in the Baltic Sea. Polar Rec. 490 (1), 33–41.

Li, F., Goerlandt, F., Kujala, P., Lehtiranta, J., Lensu, M., 2018. Evaluation of selected state-of-the-art methods for ship transit simulation in various ice conditions based on full-scale measurement. Cold Reg. Sci. Technol. 151, 94–108. https://doi.org/10.1016/j.coldregions.2018.03.008. ISSN 0165-232X. (URL).

Lindqvist, G., 1989. A straightforward method for calculation of ice resistance of ships. In: The 10th International Conference on Port and Ocean Engineering under Arctic Conditions (POAC), pp. 722–735.

Liu, J., Lau, M., Williams, F.M., 2006. Mathematical modeling of ice-hull interaction for ship maneuvering in ice simulations. In: Proceedings of 7th International Conference and Exhibition on Performance of Ships and Structures in Ice (ICETECH), Banff, Alberta, Canada.

Liu, X., Sattar, S., Li, S., 2016. Towards an automatic ice navigation support system in the Arctic sea. ISPRS Int. J. Geo Inform. 50 (3), 36. https://doi.org/10.3390/ijgi5030036. mar ISSN 2220–9964. URL.

Löptien, U., Dietze, H., 2014. Sea ice in the Baltic Sea – revisiting BASIS ice, a historical data set covering the period. Earth Syst. Sci. Data 6, 367–374. https://doi.org/10.5194/essd-6-367-2014. URL.

Lu, L., Goerlandt, F., Banda, O.A.V., Kujala, P., Höglund, A., Arneborg, L., 2019. A bayesian network risk model for assessing oil spill recovery effectiveness in the ice-covered northern Baltic Sea. Mar. Pollut. Bull. 139, 440–458.

Lubbad, R., Løset, S., 2011. A numerical model for real-time simulation of ship–ice interaction. Cold Reg. Sci. Technol. 650 (2), 111–127 (Feb).

Madkour, A., Aref, W.G., Rehman, F.U., Rahman, M.A., Basalamah, S., 2017. A Survey of Shortest-Path Algorithms. arXiv preprint arXiv:1705.02044. .

Mellor, M., 1980. Ship resistance in thick brash ice. Cold Reg. Sci. Technol. 30 (4), 305–321 (Aug).

Montewka, J., Goerlandt, F., Kujala, P., Lensu, M., 2015. Towards probabilistic models for the prediction of a ship performance in dynamic ice. Cold Reg. Sci. Technol. 1120 (Supplement C), 14–28 (Apr).

Montewka, J., Guinness, R., Kuuliala, L., Goerlandt, F., Kujala, P., Lensu, M., 2018. Challenges in modelling characteristics of maritime traffic in winter conditions and new solution proposal. In: Guedes Soares, C., Teixeira, A. (Eds.), *Developments in Maritime Transportation and Exploitation of Sea Resources - Proceedings of IMAM 2017, 17th International Congress of the International Maritime Association of the Mediterranean*, Pages 247–256. CRC Press. Taylor&Francis Group, London.

Montewka, J., Goerlandt, F., Lensu, M., Kuuliala, L., Guinness, R.E., 2019. Towards a hybrid model of ship performance in ice suitable for route planning purpose. Proc. Inst. Mech. Eng. Part O 2330 (1), 18–34.

Mussells, O., Dawson, J., Howell, S., 2017. Navigating pressured ice: risks and hazards for winter resource-based shipping in the Canadian arctic. OceanCoast. Manage. 137, 57–67.

Nam, J.-H., Park, I., Lee, H.J., Kwon, M.O., Choi, K., Seo, Y.-K., 2013. Simulation of optimal arctic routes using a numerical sea ice model based on an ice-coupled ocean circulation method. Int. J. Naval Architect. Ocean Eng. 50 (2), 210–226. ISSN 2092–6782. jun. https://doi.org/10.3744/JNAOE.2013.5.2.210 (URL).

Piehl, H., Milakovic, A.-S., Ehlers, S., 2017. A finite element method-based potential theory approach for optimal ice routing. J. Offshore Mech. Arctic Eng. 1390 (6), 061502 Aug. (ISSN 0892-7219. doi: 10.1115/1.4037141. URL).

Reimer, N., 2015. Ship Trial for Testing of an Ice Route Optimization System.

Riska, K., 1997. Performance of merchant vessels in ice in the Baltic. Forskningsrapport / Styrelsen för vintersjöfartsforskning 52 72 pages.

Rosenblad, M., 2007. Increasing the Safety of Icebound Shipping–WP4 Operative Environment (Icebreaker Operations). *Helsinki University of Technology*. Espoo, Finland.

Rosso, M., 1989. Concentration gradient approach to continuum percolation in two dimensions. J. Phys. A Math. Gen. 220 (4), L131.

Schütz, P., 2014. Dynamic Routing through Waters Partially Covered with Sea Ice. OTC Arctic Technology Conference.

Schütz, P., et al., 2014. Dynamic routing through waters partially covered with sea ice. In: *OTC Arctic Technology Conference*. Offshore Technology Conference.

Serra, J., 1983. Image Analysis and Mathematical Morphology. Academic Press, Inc.

Stentz, A., 1994. Optimal and efficient path planning for partially-known environments. In: *Robotics and Automation, 1994. Proceedings., 1994 IEEE International Conference on*, pages 3310–3317, IEEE.

Stoddard, M.A., Etienne, L., Fournier, M., Pelot, R., Beveridge, L., 2016. Making sense of arctic maritime traffic using the polar operational limits assessment risk indexing system (POLARIS). IOP Conf. Ser. 340 (1), 012034 May.

Takagi, T., Tateyama, K., Ishiyama, T., 2014. Obstacle avoidance and path planning in ice sea using probabilistic roadmap method. In: Proceedings of the 22nd IAHR International Symposoum on Ice, pp. 510–517 Singapore.

Valdez Banda, O.A., Goerlandt, F., Montewka, J., Kujala, P., June 2015. A risk analysis of winter navigation in finnish sea areas. Accid. Anal. Prev. 79, 100–116.

Valdez Banda, O.A., Goerlandt, F., Kuzmin, V., Kujala, P., Montewka, J., July 2016. Risk management model of winter navigation operations. Mar. Pollut. Bull. 1080 (1), 242–262.

Valkonen, J., Riska, K., 2014. Assessment of the feasibility of the arctic sea transportation by using ship ice transit simulation. In: ASME 2014 33rd International Conference on Ocean, Offshore and Arctic Engineering. American Society of Mechanical Engineers.

Wróbel, K., Montewka, J., Kujala, P., 2018. System-theoretic approach to safety of remotely-controlled merchant vessel. Ocean Eng. 152, 334–345.

Zvyagin, P., Voitkunskaia, A., 2016. Model of transit transport in arctic based on graph algorithms. In: ASME 2016 35th International Conference on Ocean, Offshore and Arctic Engineering. American Society of Mechanical Engineers V008T07A002–V008T07A002.